

Article

# The Influence of Surface Radiation on the Passive Cooling of a Heat-Generating Element

Igor V. Miroshnichenko <sup>1,\*</sup>, Mikhail A. Sheremet <sup>2</sup> and Abdulmajeed A. Mohamad <sup>3</sup>

<sup>1</sup> Regional Scientific and Educational Mathematical Centre, Tomsk State University, 634050 Tomsk, Russia

<sup>2</sup> Laboratory on Convective Heat and Mass Transfer, Tomsk State University, 634050 Tomsk, Russia; sheremet@math.tsu.ru

<sup>3</sup> Department of Mechanical and Manufacturing Engineering, Schulich School of Engineering, CEERE, The University of Calgary, Calgary, AB T2N 1N4, Canada; mohamad@ucalgary.ca

\* Correspondence: miroshnichenko@mail.tsu.ru; Tel.: +7-3822-529740

Received: 21 February 2019; Accepted: 9 March 2019; Published: 13 March 2019



**Abstract:** Low-power electronic devices are suitably cooled by thermogravitational convection and radiation. The use of modern methods of computational mechanics makes it possible to develop efficient passive cooling systems. The present work deals with the numerical study of radiative-convective heat transfer in enclosure with a heat-generating source such as an electronic chip. The governing unsteady Reynolds-averaged Navier–Stokes (URANS) equations were solved using the finite difference method. Numerical results for the stream function–vorticity formulation are shown in the form of isotherm and streamline plots and average Nusselt numbers. The influence of the relevant parameters such as the Ostrogradsky number, surface emissivity, and the Rayleigh number on fluid flow characteristics and thermal transmission are investigated in detail. The comparative assessment clearly emphasizes the effect of surface radiation on the overall energy balance and leads to change the mean temperature inside the heat generating element. The results of the present study can be applied to the design of passive cooling systems.

**Keywords:** convection; local heat-generating element; surface radiation; Ostrogradsky number; finite difference method

## 1. Introduction

Numerical and experimental studies on turbulent thermogravitational convection with surface radiation represent a highly topical issue for investigators due to its vast applicability in various technological applications that include electronic cooling, heat exchangers, thermal insulation systems, etc. The cooling of electronic components which are located in closed electronic cabinets remains a large problem for researchers due to the constant miniaturization of these components and the increasing level of operating temperatures. Thermogravitational convection cooling is very suitable, because it does not assume any fans which may break down. Moreover, passive convective cooling is also reliable, inexpensive, and quiet. The efficient optimization and thorough design of electronic devices require modern experimental and numerical approaches.

In the last decades, a significant number of papers have been published in specialized literature concerning the problem under consideration [1–4]. An excellent review on thermogravitational convection in enclosures for engineering applications was presented by Bairy et al. [5]. They studied a wide variety of configurations of cavities with different inclinations and shapes, heat source distributions, initial conditions, thermal boundary conditions, radiative properties, and nature of the fluid. In many practical situations, if either the characteristic dimension of the enclosure or the temperature difference is large enough, the fluid motion becomes turbulent in nature. Miroshnichenko

and Sheremet [6] presented a comprehensive review of main results in the field of turbulent thermogravitational convection with and without radiation in rectangular cavities. That study also indicated that the effects of radiation on thermal transmission and liquid circulation required investigation. A detailed review of the literature on the entropy generation analysis for heat transfer processes involving various practical applications was performed by Biswal and Basak [7].

Baudoin et al. [8] investigated the optimized distribution of a significant number of power electronic devices cooled by turbulent thermogravitational convection. The authors tried to evaluate the distribution of up to 36 flush-mounted rectangular heat sources to give the best possible cooling capacity. They studied the effect of turbulence on the optimal (i.e., minimal temperature rise for a given area) distribution of heaters. Tou et al. [9] performed a numerical study of thermogravitational convection cooling on a 3-by-3 array of discrete heat sources on one vertical wall of a rectangular enclosure and cooled by the opposite wall. It was found that heat transfer from discrete heaters was non-uniform and should be accounted for by applying the averaging techniques. They also found that the effects of the Prandtl number were negligible in the range from 5 to 130. The paper presented by Bondarenko et al. [10] was devoted to the numerical simulation of free convection of the nanofluid cooling of heat-generating and heat-conducting sources using the heatline visualization technique. They concluded that the addition of nanoparticles could enhance the cooling process for the electronic devices for various distances between the heat source and cold wall. A numerical investigation of laminar unsteady thermogravitational convection in a closed enclosure having a local heat source of different geometric shapes was performed by Gibanov and Sheremet [11]. They considered heat source shapes which illustrated a smooth transition from rectangular cross-section to a triangular one through trapezoidal forms. Thermogravitational convection combined with thermal radiation in an air-filled rectangular enclosure with a discrete heater was studied by Saravanan and Sivaraj [12]. It was found that the global heat transfer rate was enhanced with an increase in the Rayleigh number and of the emissivity of the surface for both the heat generating and the isothermal heat sources. Sheremet et al. [13] investigated natural convection thermal transmission in a partially open alumina-water nanoliquid area under the effect of vertical solid mural and local heat-generating source. They concluded that the influence of nano-sized alumina particles was more significant in the case of low intensive liquid circulation and when the heat source was located near the cooling wall.

To simplify modeling of heat and mass transfer processes, radiation is generally ignored owing to the expected low temperatures. Nevertheless, over the past decade, refined computations as well as some reduced scale experiments have shown that thermal radiation can have a big impact on fluid flow characteristics and thermal transmission even at relatively insignificant temperature levels. A series of numerical experiments considering thermogravitational convection with radiative thermal transmission at large temperature differences in a rectangular cavity with a heated cylinder at its center were performed by Parmananda et al. [14]. They showed that square geometry was the optimum design of a heated cylinder as it had minimum entropy generation and maximum heat transfer. A similar numerical study of combined radiative-convective heat transfer in a three-dimensional differentially heated cavity was carried out by Parmananda et al. [15]. Dehbi et al. [16] investigated the effect of thermal radiation on thermogravitational convection inside enclosures. Numerical experiments were conducted with and without consideration of the gas radiation heat transfer. It should be mentioned that including radiation significantly improves the prediction of the flow field. Turbulent modes of convection and radiation in an air-filled differentially-heated enclosure at  $Ra = 1.5 \times 10^9$  were studied by Ibrahim et al. [17]. They conducted a comparative analysis for four cases (only gas radiation, only wall radiation, combined gas with wall radiation, and without radiation) and compared them in terms of temperature and velocity fields as well as turbulent quantities (turbulence intensity and kinetic energy). Their findings indicated that gas radiation had a little influence on the flow structure, at least when considered alone (without wall radiation). The work of Sharma et al. [18] was devoted to the turbulent thermogravitational convection in a rectangular enclosure with symmetrical cooling from the vertical side walls and localized heating from below. It should be noted that correlations have been

developed to evaluate the Nusselt number in terms of the Rayleigh number and the heated width. The effect of rotating a square cavity with a heater was investigated by Mikhailenko et al. [19]. They tried to find optimal conditions for the heated devices in order to decrease the working temperature of these elements. One main result of that work was that an intensive rotation could essentially reduce the average temperature inside a local heat-generating source.

The effect of enclosure shapes on thermal transmission and fluid flow has received considerable attention in the recent past [20]. Das et al. [21] presented a review of the results of studies on free convection in enclosures of various shapes. That work summarized the research on convection heat transfer in trapezoidal, triangular, and parallelogrammic cavities and cavities with wavy and curved walls. The mentioned results demonstrated possible strategies for improving the efficiency of convective heat transfer. Kang et al. [22] experimentally investigated vertical tubes with inverted triangular fins under thermogravitational convection. The influence of different fin heights, fin numbers, and heat inputs was studied. They proposed the Nusselt number correlation, which has the potential of being used in the tube design of various cooling devices. Free convection inside a square system containing two vertical thin heat-generating baffles was analyzed by Saravanan and Vidhya Kumar [23]. They focused mainly on investigating the effect of various positions of the baffles and different boundary conditions on the vertical walls.

To the best of the authors' knowledge, the problem of turbulent convective-radiative heat transfer inside cavities with heat-generating sources has not been well understood. The cavity configuration under consideration is quite important for the electronics industry where similar basic designs are used. Numerical simulations were performed for various surface emissivities of walls, Rayleigh numbers, and Ostrogradsky numbers. The aim of the analyses of thermal transmission was also to investigate the Nusselt number distribution on the heat source surface.

## 2. Governing Equations and Numerical Method

The present work considered a turbulent flow of Newtonian fluid (air) under the condition of a transparent medium. Solid walls and a heater were assumed to be opaque, gray, and diffuse emitters. The Boussinesq approximation was used to describe the density changes. It was assumed in the analysis that the fluid was viscous, heat conducting, and Newtonian. Using air as the working fluid inside the enclosure and the real wall material allowed us to consider that the thermophysical properties of the fluid were independent of temperature. The physical system is defined in Figure 1. In the present model, a heat-generating source is located at the bottom wall of the enclosure with length of  $0.2L$  and has an internal constant volumetric heat flux  $Q$ . The external surfaces of the top wall ( $y = L + 2l$ ), right wall ( $x = L + 2l$ ), and left wall ( $x = 0$ ) are maintained under conditions of convective heat exchange with an environment. Remaining external surface ( $y = 0$ ) is adiabatic. No-slip boundary conditions are supposed for the internal walls of the cavity.

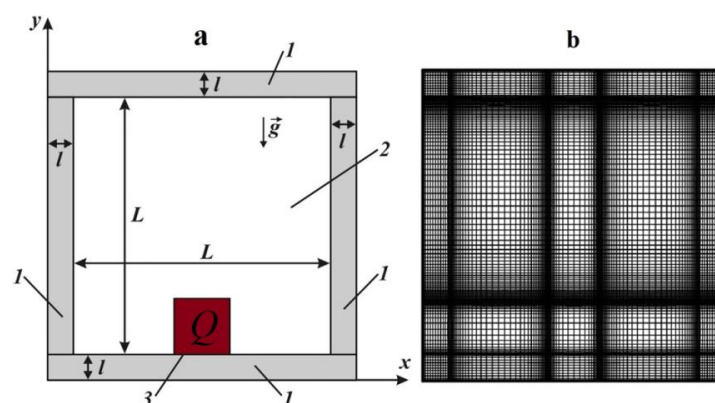


**Figure 1.** (a) A schematic of the system: 1—solid walls, 2—air, 3—heat-generating element; (b) computational domain with a non-uniform grid.

From time  $t > 0$ , there is a temperature difference between the fluid and various surfaces. The thermodynamic equilibrium is disturbed by the appearance of buoyancy forces. Bearing in mind the above assumptions, the Reynolds-averaged Navier–Stokes equations can be written in the following form:

$$\frac{\partial G}{\partial t} + \frac{\partial S_1}{\partial x_1} + \frac{\partial S_2}{\partial x_2} = R, \quad (1)$$

$$G = \begin{pmatrix} 0 \\ u_1 \\ u_2 \\ T_f \\ k \\ \epsilon \\ T_w \\ T_{hs} \end{pmatrix}, \quad (2)$$

$$S_i = \begin{pmatrix} u_i \\ p\delta_{i1} - (v + \nu_t)\sigma_{i1} + u_i u_1 \\ p\delta_{i2} - (v + \nu_t)\sigma_{i2} + u_i u_2 \\ -(\alpha + \alpha_t)\partial T_f / \partial x_i + u_i T_f \\ -(v + \nu_t / \sigma_k)\partial k / \partial x_i + u_i k \\ -(v + \nu_t / \sigma_\epsilon)\partial \epsilon / \partial x_i + u_i \epsilon \\ \alpha_w \partial T_w / \partial x_i \\ \alpha_{hs} \partial T_{hs} / \partial x_i \end{pmatrix}, \quad \forall i = 1, 2, \quad (3)$$

$$R = \begin{pmatrix} 0 \\ 0 \\ g\beta\Delta T \\ 0 \\ P_k + G_k - \epsilon \\ (c_{1\epsilon}(P_k + c_{3\epsilon}G_k) - c_{2\epsilon}\epsilon)\frac{\epsilon}{k} \\ 0 \\ q_v \end{pmatrix}, \quad (4)$$

$$\sigma_{ij} = \frac{\partial u_i}{\partial x_j} + \frac{\partial u_j}{\partial x_i}, \quad (5)$$

where  $P_k$  describes the production of  $k$ ,  $G_k$  defines the generation or dissipation of turbulent kinetic energy due to buoyancy, and these terms are expressed as

$$P_k = \nu_t \left[ 2 \left( \frac{\partial u_1}{\partial x_1} \right)^2 + 2 \left( \frac{\partial u_2}{\partial x_2} \right)^2 + \left( \frac{\partial u_1}{\partial x_2} + \frac{\partial u_2}{\partial x_1} \right)^2 \right], \quad G_k = -\frac{g\beta\nu_t}{Pr_t} \frac{\partial T}{\partial x_2}. \quad (6)$$

In the present study, the  $k$ - $\epsilon$  model was used to describe the Reynolds stress terms [24,25]. For completeness of information, the following expressions adopted to define the closure coefficients of the turbulence model (i.e.,  $c_\mu$ ,  $c_{1\epsilon}$ ,  $c_{2\epsilon}$ ,  $c_{3\epsilon}$ ,  $\sigma_k$ ,  $\sigma_\epsilon$ , and  $Pr_t$ ) are summarized in Table 1. To make this problem dimensionless, the reference parameters  $V_0 = \sqrt{g\beta\Delta TL}$ ,  $t_0 = \sqrt{g\beta\Delta T/L}$ , and  $L$  which, respectively, represent the velocity, time, and length are used. The following dimensionless variables are given as follows:

$$X = x_1/L, Y = x_2/L, \tau = t\sqrt{g\beta\Delta T/L}, U = u_1/\sqrt{g\beta\Delta TL}, V = u_2/\sqrt{g\beta\Delta TL}, \Theta = (T - T^e)/(T_0 - T^e), \\ \Psi = \psi/\sqrt{g\beta\Delta TL^3}, \Omega = \omega\sqrt{L/g\beta\Delta T}, K = k/(g\beta\Delta TL), E = \epsilon/\sqrt{g^3\beta^3(\Delta T)^3L}$$

**Table 1.** Empirical constants for the turbulence model.

Parameters	$c_\mu$	$c_{1\epsilon}$	$c_{2\epsilon}$	$c_{3\epsilon}$	$\sigma_k$	$\sigma_\epsilon$	$Pr_t$
Values	0.09	1.44	1.92	0.8	1.0	1.3	1.0

In order to investigate the fluid flow in terms of streamlines, the dimensionless vorticity and stream function can be calculated in the usual way as follows:

$$\Omega = \frac{\partial V}{\partial X} - \frac{\partial U}{\partial Y}, \quad U = \frac{\partial \Psi}{\partial Y}, \quad V = -\frac{\partial \Psi}{\partial X}. \quad (7)$$

The thermal transmission and liquid circulation are determined by the following governing parameters: the Ostrogradsky number ( $Os$ ), the Prandtl number ( $Pr$ ), and the Rayleigh number ( $Ra$ ). They are defined, respectively, in the following form:

$$Os = \frac{q_v L^2}{\lambda_{hs} \Delta T}, \quad Pr = \frac{\nu}{\alpha_f}, \quad Ra = \frac{g \beta \Delta T L^3}{\nu \alpha_f}. \quad (8)$$

The initial conditions for the non-dimensional governing equations are considered in the following form:

$$\Psi(X, Y, 0) = \Omega(X, Y, 0) = K(X, Y, 0) = E(X, Y, 0) = 0, \quad \Theta(X, Y, 0) = 1.0 \text{ at } \tau = 0.$$

The boundary conditions are expressed as follows:

For the energy equations:  $\frac{\partial \Theta}{\partial Y} = 0$  at  $Y = 0$ ;  $\frac{\partial \Theta}{\partial \bar{n}} = Bi \cdot \Theta$  at  $X = 0, X = 1 + 2l/L, Y = 1 + 2l/L$ ;  $\Theta_1 = \Theta_2, \frac{\partial \Theta_w}{\partial \bar{n}} = \frac{\lambda_f}{\lambda_w} \frac{\partial \Theta_f}{\partial \bar{n}} - N_{rad} Q_{rad}$  at internal solid–fluid interfaces; and  $\frac{\partial \Theta_{hs}}{\partial \bar{n}} = \frac{\lambda_f}{\lambda_{hs}} \frac{\partial \Theta_f}{\partial \bar{n}} - N_{rad} Q_{rad}$  at the heat-generating source surface.

For the momentum equations:  $\Psi = \frac{\partial \Psi}{\partial \bar{n}} = 0, \Omega = -\frac{\partial^2 \Psi}{\partial \bar{n}^2}$  at internal solid–fluid interfaces.

The boundary conditions for the turbulent parameters have been described in detail previously in [24]. To change a non-uniform grid in physical domain to a uniform grid in computational domain, a special algebraic coordinate transformation has been applied [24,25].

In this paper, the surfaces were assumed to be gray. The process of radiative heat exchange between such surfaces (due to absorption and reflection) is complicated compared to the same process for absolutely black bodies. Radiation analysis has been carried out using the balance method [24–26]. To receive the dimensionless net radiative heat flux  $Q_{rad}$ , it is necessary to solve the following equations:

$$Q_{rad,k} = R_k - \sum_{i=1}^N F_{k-i} R_i, \quad (9)$$

$$R_k = (1 - \tilde{\epsilon}_k) \sum_{i=1}^N F_{k-i} R_i + \tilde{\epsilon}_k (1 - \zeta)^4 \left( \Theta_k + 0.5 \frac{1 + \zeta}{1 - \zeta} \right)^4. \quad (10)$$

The contribution of radiation is a significant topic for heat transfer in enclosures. Radiation heat transfer depends on various parameters such as the wall temperature, surface emissivity, cavity geometry, and thermophysical properties of the internal medium. In studies focused on thermogravitational convection, the radiative mode of heat transfer is sometimes neglected due to the suppressing number of computational resources it demands. At the same time, as practice shows, radiation has a significant impact on the system under consideration and cannot be neglected. Thus, real materials will emit (and consequently absorb) less thermal radiation than predicted for a black body. In the present work, the internal surfaces of the heat source and all walls were considered to be both gray diffusive emitters and reflectors of radiation. The air flow inside the enclosure was considered

radiatively non-participating. The parameter  $\tilde{\epsilon}$  (which varies in this work) was also reasonable from a physical point of view.

The finite difference method was used to solve the set of governing equations. The diffusion terms were discretized using the second-order accurate central difference scheme, whereas the accurate upwind difference scheme was used for the convective terms. The Samarskii locally one-dimensional scheme was adopted to solve the parabolic equations. The first-order upwind scheme was used for the discretization of the transient term. The resulting systems of linear equations were solved using the Thomas algorithm. The elliptical equation was discretized using the second-order accurate central differencing scheme. The successive over-relaxation method was used to solve the obtained difference equation. The time step used here was chosen to be  $\Delta t = 10^{-4}$ . A numerical code was written in C++ programming language. The case of surface radiation and thermogravitational convection in a differentially heated air-filled square cavity was investigated to validate the numerical procedure. The obtained results were compared with the numerical data of Wang et al. [27]. Figures 2 and 3 show a good agreement between the data under consideration (maximum deviation in parameters is 10%).

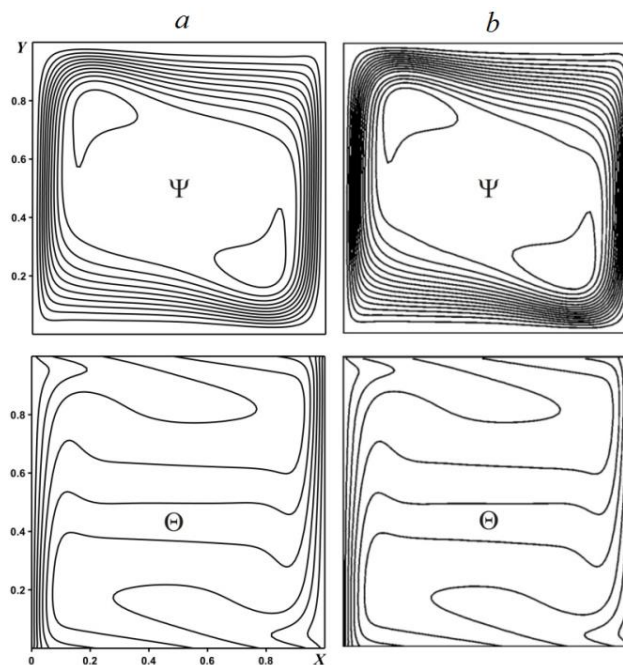


**Figure 2.** (a) Streamlines  $\Psi$  and isotherms  $\Theta$  at  $Ra = 10^6$ ,  $\tilde{\epsilon} = 0.8$  (b) numerical data of Wang et al. [27].

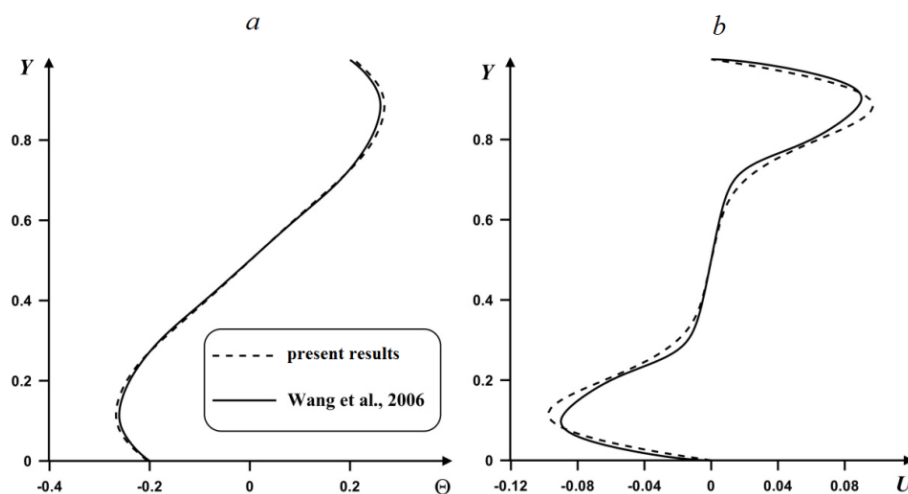


**Figure 3.** Profiles of (a) temperature and (b) horizontal velocity at  $X = 0.5$  at  $Ra = 10^6$ ,  $\tilde{\epsilon} = 0.2$  in comparison with numerical data of Wang et al. [27].

In the case of thermogravitational convection in the enclosure, the developed computational code was validated successfully using the numerical results of Dixit and Babu [28], Zhuo and Zhong [29], and Le Quéré [30] (see Table 2). The numerical simulation was carried out on finer and coarser meshes to check the grid independence. These computational tests with various grids allowed choosing the suitable grid size selection without compromising CPU time and accuracy. The average convective Nusselt number on the heat source surface, fluid flow rate, and average heater temperature are shown in Table 3. Therefore, the grid of  $120 \times 120$  nodes was chosen for further investigation.

**Table 2.** Variation of the average Nusselt numbers.

$Ra$	Dixit et al. [28]	Zhuo et al. [29]	Le Quéré [30]	Present Data
$10^7$	16.79	16.523	–	17.13
$10^8$	30.506	30.225	28.78	33.06
$10^9$	57.35	–	62.0	60.54

**Table 3.** Grid independence study for  $Ra = 10^9$ ,  $\tilde{\epsilon} = 0$ ,  $\tau = 1000$ .

Grid Size	$\delta$	$Nu_{conv}$	$ \psi _{\max}$	$\Theta_{hs}$
$60 \times 60$	$5.7 \times 10^{-3}$	48.78	0.031	0.764
$120 \times 120$	$2.5 \times 10^{-3}$	61.54	0.028	0.783
$156 \times 156$	$1.9 \times 10^{-3}$	64.974	0.027	0.786

It should be noted that the optimum over-relaxation parameter for the elliptical equation was found to be 1.9. Simple, but at the same time thorough criteria for each of the variables were used to obtain converged solutions at each time step. The convergence condition  $|\beta_{ij}^{k+1} - \beta_{ij}^k| < 10^{-6}$  must be satisfied by each variable  $\beta_{ij}^k$  at any grid point  $(i, j)$ ; here,  $k$  is a given iteration parameter.

### 3. Results

The main aim of this work was to analyze the effect of surface radiation as well as the Ostrogradsky and Rayleigh numbers variation on fluid flow characteristics and thermal transmission. In this section, the numerical results are reported for  $0.1 < Os < 2$ ,  $Ra = 10^8$ ,  $Ra = 10^9$ ,  $Ra = 10^{10}$ . The various values of surface emissivity (0, 0.3, 0.6, and 0.9) of the heat-generating source and the solid wall surfaces were used to examine the influence of radiation on convective heat exchange. Air ( $Pr = 0.71$ ) was the working fluid. It should be noted that the thermal conductivity of the heater material  $\lambda_{hs}$  corresponded to the value of silicon. The thermal conductivity of the solid walls  $\lambda_w$  was specially selected with a small value of 0.7. Numerical results for the various Nusselt numbers ( $Nu_{con}$  and  $Nu_{rad}$ ) for different conditions are represented and discussed. The geometry was selected in order to simulate the cooling of an electronic device located on a bottom horizontal surface. The results were obtained using one Intel Core i7 processor of 3.30 GHz with 16GB of RAM memory.

Figure 4 shows two-dimensional temperature fields at  $Ra = 10^8$ ,  $Os = 1$ ,  $\tilde{\epsilon} = 0.6$  for various values of the dimensionless time. At the initial time ( $\tau = 3$ ), the distributions of temperature reflect the formation of two small thermal plumes over the heat-generating source. It is worth noting that heat conduction is the governing mechanism of heat transfer near the heater due to low convective velocity at initial time. At  $\tau = 10$ , the thermal plumes' height is about a third of the enclosure height, and further on ( $\tau = 15$ ) a single thermal plume is formed. The ascending hot air reaches an internal surface of the top wall, while close to the internal surfaces of two vertical walls the descending flow is formed. Subsequently, the dimensionless time increasing leads to more intensive low temperature penetration from the environment.

The effect of surface-to-surface radiation (non-participating gas medium) was investigated. Isotherms  $\Theta$  and streamlines  $\Psi$  are shown in Figure 5 for the various surface emissivities of the heater and solid walls. It can be seen that two convective cells (with counterclockwise and clockwise

rotating) are observed for all the values of  $\tilde{\epsilon}$ . The fluid due to heat transport from the heat-generating source rises up and collides at the top adiabatic wall; further on, it bifurcates and flows to the solid vertical walls. Thus, the convective cells have nearly equal strength. The strength of these vortices increases (see Figure 5) with a decreasing value of surface emissivity. Therefore, an insignificant intensification of the fluid flow in the enclosure  $|\Psi|_{\max}^{\tilde{\epsilon}=0.9} = 0.021$ ,  $|\Psi|_{\max}^{\tilde{\epsilon}=0.3} = 0.022$ ,  $|\Psi|_{\max}^{\tilde{\epsilon}=0.0} = 0.023$  is observed with a reduction of  $\tilde{\epsilon}$ . At the same time, the temperature fields are changed more significantly. Inside the enclosure, an increase in  $\Theta$  is observed. In particular, it can be seen in isotherm ( $\Theta = 0.6$ ) which is located above the heater ( $\tilde{\epsilon} = 0$ ) that it is further ascended with a thermal plume ( $\tilde{\epsilon} = 0.9$ ). These numerical results are confirmed by the observations made by Martyushev and Sheremet [31] in the laminar case.

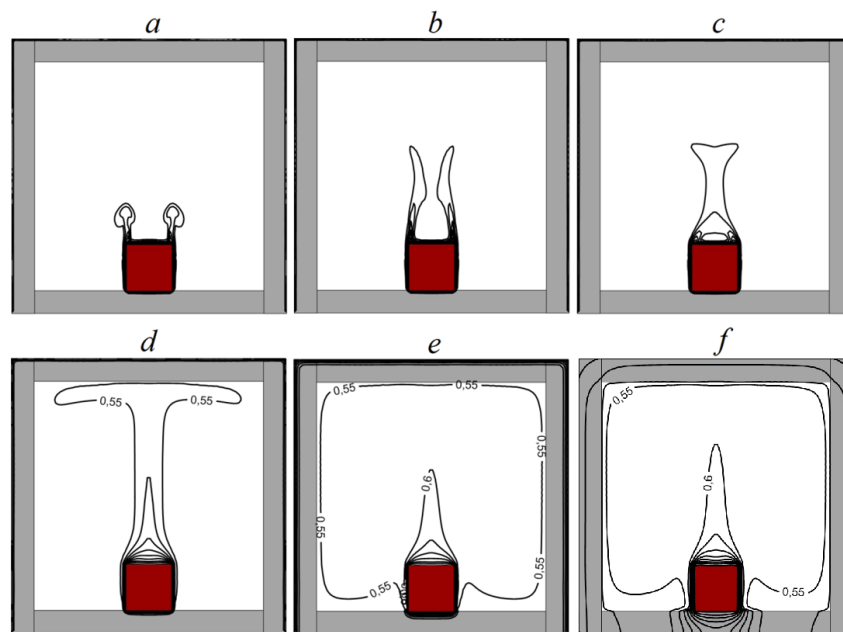


**Figure 4.** Isotherms  $\Theta$  at  $Ra = 10^9$ ,  $Os = 1$ ,  $\tilde{\epsilon} = 0.3$ : (a)  $\tau = 3$ , (b)  $\tau = 10$ , (c)  $\tau = 15$ , (d)  $\tau = 50$ , (e)  $\tau = 200$ , and (f)  $\tau = 2000$ .

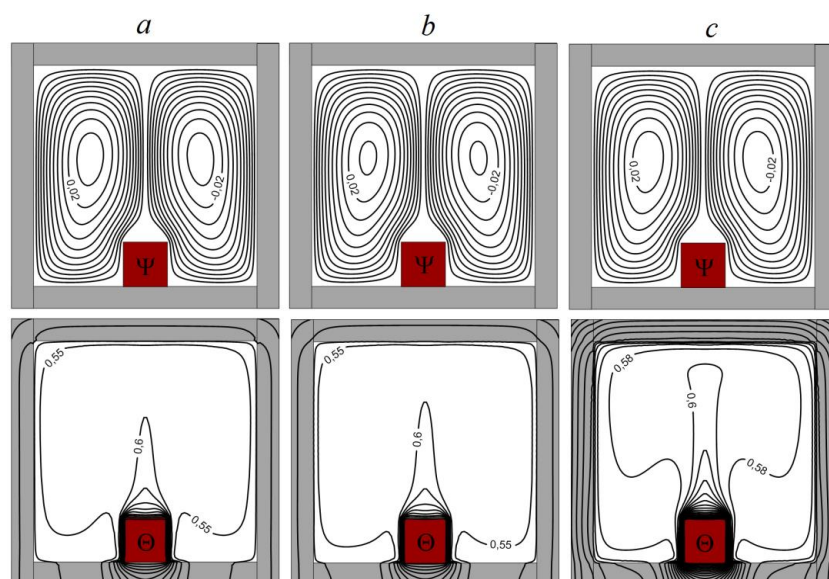


**Figure 5.** Isotherms  $\Theta$  and streamlines  $\Psi$  at  $Ra = 10^9$ ,  $Os = 1$ ,  $\tau = 2000$ : (a), (b)  $\tilde{\epsilon} = 0.3$ , and (c)  $\tilde{\epsilon} = 0.9$ ,  $\tilde{\epsilon} = 0$ .

In order to study the effect of radiation on thermal transmission, the total heat transfer from the heater was evaluated using the mean radiative and convective Nusselt numbers. Figure 6 depicts  $Nu_{conv}$  and  $Nu_{rad}$  at the fluid–solid interfaces for various values of surface emissivity. The presented results indicate that there is no time point which characterizes the stationary distribution of heat transfer coefficients. It is caused by permanent heat generation at the local heater. Thus, surface emissivity enhances the mean radiative Nusselt number by 2.84 times upon the change of  $\tilde{\epsilon}$  from 0.3 to 0.9. Due to a decrease in the temperature gradient, a growth of  $\tilde{\epsilon}$  leads to the reduction of the mean convective Nusselt number. However, this change is minor.

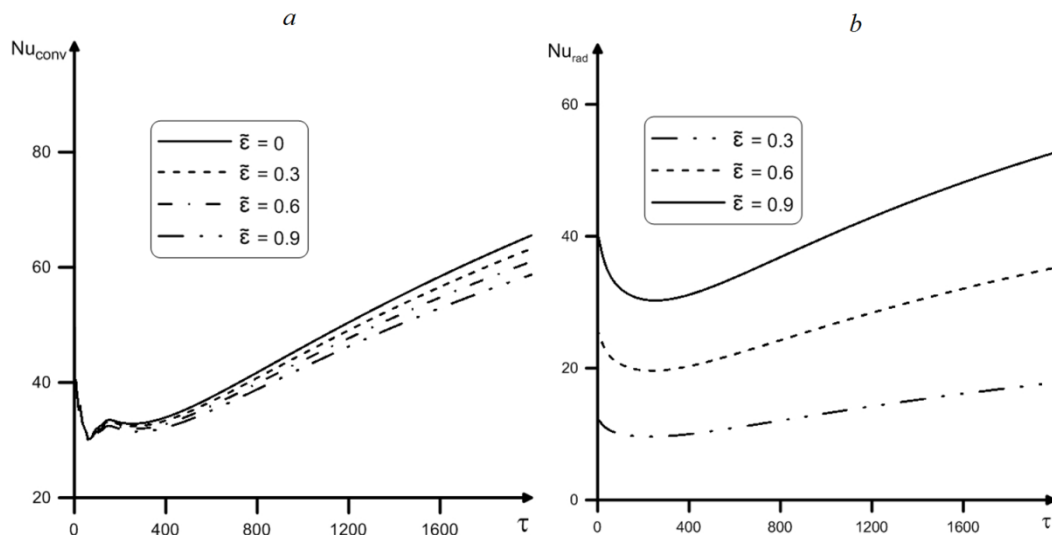


**Figure 6.** Dependences of the mean (a) convective and (b) radiative Nusselt numbers at the heat-generating source surface vs. surface emissivity and dimensionless time at  $Ra = 10^9$ ,  $Os = 1$ .

A more detailed impact of the surface emissivity on the temperature profiles at the middle cross-section  $X = 0.6$  is depicted in Figure 7. The main focus was on investigating the effect of radiation on the temperature field in a heat-generating source. An in-depth analysis of this problem allowed us to better understand the principles of passive cooling of electronic elements. It should be noted that the growth of surface emissivity was manifested in a noticeable decrease in temperature inside the local heater. This fact was also expressed in a more intensive cooling of the top heat-conducting wall and, consequently, an increase in the temperature gradient on the surface of this wall. It is clear that the consideration of surface radiation modifies the temperature fields substantially.

Table 4 demonstrates variations of various considered parameters (average temperature inside the air cavity, maximum absolute value of the stream function, average temperature inside the heat-generating source) for  $Ra = 10^8$ ,  $Os = 1$ . An increment of surface emissivity value reduces  $|\psi|_{\max}$  due to a decrease in the convective flow in the enclosure. A growth of  $\tilde{\epsilon}$  allows the reduction of the average temperature inside the heater and, at the same time, leads to a slight increase in the mean temperature inside the enclosure.

**Table 4.** Variations of different considered parameters for  $Ra = 10^8$ ,  $\tau = 2000$ .

Surface Emissivity Value	$\Theta_{cavity}$	$ \psi _{\max}$	$\Theta_{hs}$
0	0.426	0.0349	0.9425
0.3	0.428	0.0344	0.9295
0.6	0.431	0.0339	0.9172
0.9	0.433	0.0334	0.9050

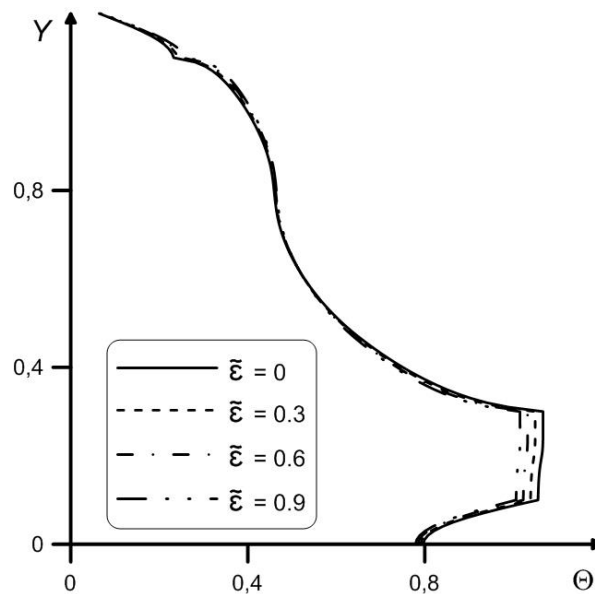


**Figure 7.** Temperature profiles at  $X = 0.6$ ,  $Ra = 10^9$ ,  $Os = 1$  and different values of surface emissivity.

When designing electronic devices, the primary interest is to always control and predict the temperature inside the enclosure. The development of new types of electronics tends to miniaturize individual heat-generating elements, which, as a rule, leads to an increase in operating temperatures and, accordingly, affects the reliability of the equipment. The Ostrogradsky number characterizes a volumetric heat source in the system. An increase in  $Os$  leads to a growth of the density of heat flux. Figure 8 shows the development of the isotherms  $\Theta$  for various values of the Ostrogradsky number. Just to clarify again, the heat transfer processes are caused by both the impact of the heat-generating source and the cooling of the given area owing to the convective heat exchange with an environment. It should be noted that the ambient temperature is less than the initial temperature of the area under consideration. A thermal plume is formed in the central part of the cavity, which characterizes the location of the ascending flows of hot air. Due to heat dissipation from the heater, the bottom solid wall is a zone least affected by the environment. It is clear that an increase in the Ostrogradsky number leads to an essential temperature growth. In particular, the isotherm of 0.5 at  $Os = 0.1$  is located above the heat-generating source in the air zone, whereas at  $Os = 2$  the considered isotherm is located close to the solid walls (due to more substantial heating).

Values of the mean radiative and convective Nusselt numbers at the heat source surface, mean temperature inside the heat source, and air flow rate inside the enclosure for different values of the Ostrogradsky number are presented in Table 5. At  $\tau = 2000$ , the mean radiative Nusselt number increases up to 2.01 times upon the change of  $Os$  from 0.5 to 2. It is worth noting that an increase in the Ostrogradsky number enhances the average temperature inside the heater up to 26%. In this regard, if the power of the energy source is high, its cooling becomes a non-trivial task.  $Nu_{conv}$  and  $|\psi|_{\max}$  are also increased with the density of heat flux, which is obvious. Finally, a parameter such as the Ostrogradsky number affects the reliability of the device, which is the main aspect for practical applications.

**Table 5.** Variations of different considered parameters for  $Ra = 10^9$ ,  $\tilde{\epsilon} = 0.6$ ,  $\tau = 2000$ .

Ostrogradsky Number	$Nu_{conv}$	$Nu_{rad}$	$ \psi _{\max}$	$\Theta_{hs}$
0.5	41.67	33.84	0.0196	0.7097
2	87.59	68.30	0.0250	0.8966

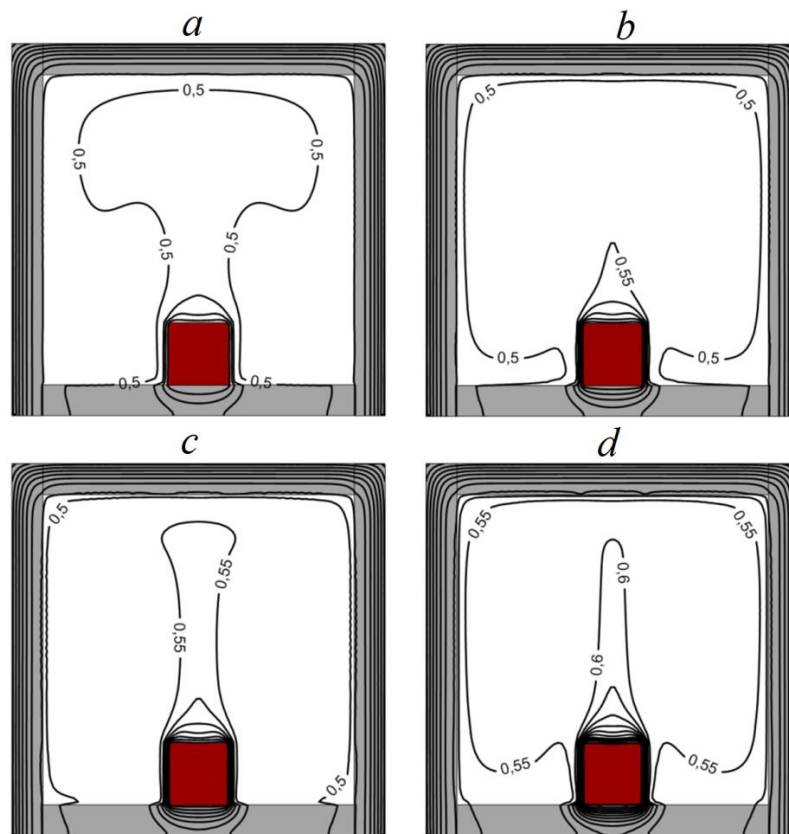


Figure 8. Isotherms  $\Theta$  at  $Ra = 10^9$ ,  $\tilde{\epsilon} = 0.6$ : (a)  $Os = 0.1$ , (b)  $Os = 0.5$ , (c)  $Os = 1$ , and (d)  $Os = 2$ .

#### 4. Conclusions

The present work was devoted to the study of the interaction of turbulent natural convection with surface radiation in an air-filled enclosure with a heat-generating source. From an engineering point of view, the considered problem is quite important for the electronics industry where similar basic designs are also used. Governing equations of energy, mass, and momentum were solved by the finite difference method. This research covered a broad range of the dimensionless parameters that were previously presented in the study. The effect of the Ostrogradsky number and surface radiation on fluid flow characteristics and thermal transmission was analyzed in detail for various combinations of the dimensionless parameters. A change in the value of  $Os$  led to either a decrease or an increase in the average heat-source temperature. It was found that the average radiative Nusselt number increased up to 2.84 times upon the change of the surface emissivity value from 0.3 to 0.9. Therefore, the surface radiation has a substantial impact on the total heat exchange and may reach 50% of the total heat flux, particularly if the heater and wall surfaces have high emissivity. In accordance with the results, it is possible to conclude that in a sealed electronic case with one heat-generating element under conditions of convective heat exchange with an environment, the heat removal from the heater can be enhanced even by a slight increase in  $\tilde{\epsilon}$ .

**Author Contributions:** I.V.M., M.A.S., and A.A.M. conceived the main concept. I.V.M., M.A.S., and A.A.M. contributed to the investigation and data analysis. I.V.M., M.A.S., and A.A.M. wrote the manuscript. All authors contributed to the writing of the final manuscript.

**Funding:** This work was supported by the Ministry of Science and Higher Education of Russia (state assignment No. 1.13557.2019/13.1).

**Acknowledgments:** The authors wish to express their thanks to the very competent reviewers for the valuable comments and suggestions.

**Conflicts of Interest:** The authors declare no conflict of interest.

## Abbreviations

$Bi = hL/\lambda_w$	Biot number
$E$	dimensionless dissipation rate of turbulent kinetic energy
$F_{k-i}$	view factor from $k$ -th element to the $i$ -th element of an enclosure
$g$	acceleration of gravity ( $\text{m/s}^2$ )
$G_k$	dimensionless generation/destruction of buoyancy turbulent kinetic energy
$h$	heat-transfer coefficient ( $\text{W/m}^2 \text{K}$ )
$k$	dimensional turbulence kinetic energy ( $\text{m}^2/\text{s}^2$ )
$K$	dimensionless turbulent kinetic energy
$l$	thickness of walls (m)
$L$	air cavity size (m)
$N_{rad} = \sigma T_{hs}^4 L / [\lambda_f (T_{hs} - T^e)]$	radiation number (or Stark number)
$Nu_{con}$	average convective Nusselt number
$Nu_{rad}$	average radiative Nusselt number
$Os = q_v L^2 / \lambda_{hs} \Delta T$	Ostrogradsky number
$p$	pressure ( $\text{N/m}^2$ )
$P_k$	dimensionless shearing production
$Pr = \nu / \alpha_f$	Prandtl number
$Pr_t = \nu_t / \alpha_t$	turbulent Prandtl number
$q_v$	volume density of heat flux ( $\text{W/m}^3$ )
$Q_{rad}$	dimensionless net radiative heat flux
$R_k$	dimensionless radiosity of the $k$ -th element of an enclosure
$Ra = g\beta(T_{hs} - T^e)L^3 / \nu\alpha_f$	Rayleigh number
$t$	dimensional time (s)
$T$	dimensional temperature (K)
$T^e$	environmental temperature (K)
$T_f$	dimensional fluid temperature (K)
$T_{hs}$	dimensional heater temperature (K)
$T_w$	dimensional wall temperature (K)
$u_1, u_2$	dimensional velocity components along $x$ and $y$ axes ( $\text{m/s}$ )
$U, V$	dimensionless velocity components along $X$ and $Y$ axes
$x_1, x_2 (x, y)$	dimensional Cartesian coordinates (m)
$X, Y$	dimensionless Cartesian coordinates
<i>Greek symbols</i>	
$\alpha_w$	thermal diffusivity of the wall material ( $\text{m}^2/\text{s}$ )
$\alpha_f$	air thermal diffusivity ( $\text{m}^2/\text{s}$ )
$\alpha_{hs}$	thermal diffusivity of the heater material ( $\text{m}^2/\text{s}$ )
$\beta$	coefficient of volumetric thermal expansion ( $1/\text{K}$ )
$\delta$	the smallest size of the mesh element
$\epsilon$	dimensional dissipation rate of turbulent kinetic energy ( $\text{m}^2/\text{s}^3$ )
$\tilde{\epsilon}$	surface emissivity
$\zeta = T^e / T_0$	temperature parameter
$\Theta$	dimensionless temperature
$\Theta_{hs}$	dimensionless heater temperature
$\Theta_f$	dimensionless temperature of fluid
$\Theta_w$	dimensionless temperature of wall
$\lambda_w$	thermal conductivity of the wall material ( $\text{W/m K}$ )
$\lambda_f$	air thermal conductivity ( $\text{W/m K}$ )
$\lambda_{hs}$	thermal conductivity of the heater ( $\text{W/m K}$ )
$\nu$	kinematic viscosity ( $\text{m}^2/\text{s}$ )
$\nu_t$	turbulent viscosity ( $\text{m}^2/\text{s}$ )
$\sigma$	Stefan–Boltzmann constant ( $\text{W/m}^2 \text{K}^4$ )

$\tau$	dimensionless time
$\psi$	dimensional stream function ( $\text{m}^2/\text{s}$ )
$\Psi$	dimensionless stream function
$\omega$	dimensional vorticity ( $\text{s}^{-1}$ )
$\Omega$	dimensionless vorticity

## References

- Xu, G.; Hu, X.; Liao, Z.; Xu, C.; Yang, C.; Deng, Z. Experimental and Numerical Study of an Electrical Thermal Storage Device for Space Heating. *Energies* **2018**, *11*, 2180. [[CrossRef](#)]
- Durgam, S.; Venkateshan, S.P.; Sundararajan, T. Experimental and Numerical Investigations on Optimal Distribution of Heat Source Array under Natural and Forced Convection in a Horizontal Channel. *Int. J. Therm. Sci.* **2017**, *115*, 125–138. [[CrossRef](#)]
- Kondrashov, A.; Sboev, I.; Dunaev, P. Evolution of Convective Plumes Adjacent to Localized Heat Sources of Various Shapes. *Int. J. Heat Mass Transf.* **2016**, *103*, 298–304. [[CrossRef](#)]
- Ridouane, E.H.; Hasnaoui, M.; Amahmid, A.; Raji, A. Interaction between Natural Convection and Radiation in a Square Cavity Heated from Below. *Numer. Heat Transf. Part A Appl.* **2004**, *45*, 289–311. [[CrossRef](#)]
- Baïri, A.; Zarco-Pernia, E.; Garcia De Maria, J.M. A Review on Natural Convection in Enclosures for Engineering Applications. the Particular Case of the Parallelogrammic Diode Cavity. *Appl. Therm. Eng.* **2014**, *63*, 304–322. [[CrossRef](#)]
- Miroshnichenko, I.V.; Sheremet, M.A. Turbulent Natural Convection Heat Transfer in Rectangular Enclosures Using Experimental and Numerical Approaches: A Review. *Renew. Sustain. Energy Rev.* **2018**, *82*, 40–59. [[CrossRef](#)]
- Biswal, P.; Basak, T. Entropy Generation vs Energy Efficiency for Natural Convection Based Energy Flow in Enclosures and Various Applications: A Review. *Renew. Sustain. Energy Rev.* **2017**, *80*, 1412–1457. [[CrossRef](#)]
- Baudoin, A.; Saury, D.; Boström, C. Optimized Distribution of a Large Number of Power Electronics Components Cooled by Conjugate Turbulent Natural Convection. *Appl. Therm. Eng.* **2017**, *124*, 975–985. [[CrossRef](#)]
- Tou, S.K.W.; Tso, C.P.; Zhang, X. 3-D Numerical Analysis of Natural Convective Liquid Cooling of a  $3 \times 3$  Heater Array in Rectangular Enclosures. *Int. J. Heat Mass Transf.* **1999**, *42*, 3231–3244. [[CrossRef](#)]
- Bondarenko, D.S.; Sheremet, M.A.; Oztop, H.F.; Ali, M.E. Natural Convection of  $\text{Al}_2\text{O}_3/\text{H}_2\text{O}$  Nanofluid in a Cavity with a Heat-Generating Element. Heatline Visualization. *Int. J. Heat Mass Transf.* **2019**, *130*, 564–574. [[CrossRef](#)]
- Gibanov, N.S.; Sheremet, M.A. Natural Convection in a Cubical Cavity with Different Heat Source Configurations. *Therm. Sci. Eng. Prog.* **2018**, *7*, 138–145. [[CrossRef](#)]
- Saravanan, S.; Sivaraj, C. Combined Thermal Radiation and Natural Convection in a Cavity Containing a Discrete Heater: Effects of Nature of Heating and Heater Aspect Ratio. *Int. J. Heat Fluid Flow* **2017**, *66*, 70–82. [[CrossRef](#)]
- Sheremet, M.; Oztop, H.; Gvozdyakov, D.; Ali, M. Impacts of Heat-Conducting Solid Wall and Heat-Generating Element on Free Convection of  $\text{Al}_2\text{O}_3/\text{H}_2\text{O}$  Nanofluid in a Cavity with Open Border. *Energies* **2018**, *11*, 3434. [[CrossRef](#)]
- Parmananda, M.; Khan, S.; Dalal, A.; Natarajan, G. Critical Assessment of Numerical Algorithms for Convective-Radiative Heat Transfer in Enclosures with Different Geometries. *Int. J. Heat Mass Transf.* **2017**, *108*, 627–644. [[CrossRef](#)]
- Parmananda, M.; Dalal, A.; Natarajan, G. Unified Framework for Buoyancy Induced Radiative-Convective Flow and Heat Transfer on Hybrid Unstructured Meshes. *Int. J. Heat Mass Transf.* **2018**, *126*, 908–925. [[CrossRef](#)]
- Dehbi, A.; Kelm, S.; Kalilainen, J.; Mueller, H. The Influence of Thermal Radiation on the Free Convection inside Enclosures. *Nucl. Eng. Des.* **2019**, *341*, 176–185. [[CrossRef](#)]
- Ibrahim, A.; Saury, D.; Lemonnier, D. Coupling of Turbulent Natural Convection with Radiation in an Air-Filled Differentially-Heated Cavity at  $\text{Ra} = 1.5 \times 10^9$ . *Comput. Fluids* **2013**, *88*, 115–125. [[CrossRef](#)]
- Sharma, A.K.; Velusamy, K.; Balaji, C. Turbulent Natural Convection in an Enclosure with Localized Heating from Below. *Int. J. Therm. Sci.* **2007**, *46*, 1232–1241. [[CrossRef](#)]

19. Mikhailenko, S.A.; Sheremet, M.A.; Mohamad, A.A. Convective-Radiative Heat Transfer in a Rotating Square Cavity with a Local Heat-Generating Source. *Int. J. Mech. Sci.* **2018**, *142–143*, 530–540. [[CrossRef](#)]
20. Shenoy, A.; Sheremet, M.; Pop, I. Convective Flow and Heat Transfer from Wavy Surfaces. In *Viscous Fluids, Porous Media, and Nanofluids*; CRC Press: Boca Raton, FL, USA, 2017.
21. Das, D.; Roy, M.; Basak, T. Studies on Natural Convection within Enclosures of Various (Non-Square) Shapes—A Review. *Int. J. Heat Mass Transf.* **2017**, *106*, 356–406. [[CrossRef](#)]
22. Kang, B.D.; Kim, H.J.; Kim, D.K. Nusselt Number Correlation for Vertical Tubes with Inverted Triangular Fins under Natural Convection. *Energies* **2017**, *10*, 1183. [[CrossRef](#)]
23. Saravanan, S.; Vidhya Kumar, A.R. Natural Convection in Square Cavity with Heat Generating Baffles. *Appl. Math. Comput.* **2014**, *244*, 1–9. [[CrossRef](#)]
24. Miroshnichenko, I.V.; Sheremet, M.A. Turbulent Natural Convection Combined with Thermal Surface Radiation inside an Inclined Cavity Having Local Heater. *Int. J. Therm. Sci.* **2018**, *124*, 122–130. [[CrossRef](#)]
25. Miroshnichenko, I.V.; Sheremet, M.A. Turbulent Natural Convection and Surface Radiation in a Closed Air Cavity with a Local Energy Source. *J. Eng. Phys. Thermophys.* **2017**, *90*, 557–563. [[CrossRef](#)]
26. Howell, J.R.; Menguc, M.P.; Siegel, R. Thermal Radiation Heat Transfer, 6th Edition. *J. Heat Transf.* **1970**. [[CrossRef](#)]
27. Wang, H.; Xin, S.; Le Quere, P. Numerical study of natural convection-surface radiation coupling in air-filled square cavities. *C. R. Mecanique* **2006**, *334*, 48–57. [[CrossRef](#)]
28. Dixit, H.N.; Babu, V. Simulation of High Rayleigh Number Natural Convection in a Square Cavity Using the Lattice Boltzmann Method. *Int. J. Heat Mass Transf.* **2006**, *49*, 727–739. [[CrossRef](#)]
29. Zhuo, C.; Zhong, C. LES-Based Filter-Matrix Lattice Boltzmann Model for Simulating Turbulent Natural Convection in a Square Cavity. *Int. J. Heat Fluid Flow* **2013**, *42*, 10–22. [[CrossRef](#)]
30. Le Quéré, P. Accurate Solutions to the Square Thermally Driven Cavity at High Rayleigh Number. *Comput. Fluids* **1991**, *20*, 29–41. [[CrossRef](#)]
31. Martyushev, S.G.; Sheremet, M.A. Conjugate Natural Convection Combined with Surface Thermal Radiation in an Air Filled Cavity with Internal Heat Source. *Int. J. Therm. Sci.* **2014**, *76*, 51–67. [[CrossRef](#)]



© 2019 by the authors. Licensee MDPI, Basel, Switzerland. This article is an open access article distributed under the terms and conditions of the Creative Commons Attribution (CC BY) license (<http://creativecommons.org/licenses/by/4.0/>).